Kovove Mater. 61 2023 145–159
DOI: 10.31577/km.2023.3.145

Effect of antimony addition on the microstructure modification and properties evolution of hypereutectic Al-Si-Zr alloy

Peng Tang[1,2,3]*, Kailai Yu[1], Xinghuai Mao[1]

[1] *School of Resources, Environment and Materials, Guangxi University, Nanning, 530004, P. R. China*
[2] *State Key Laboratory of Featured Metal Materials and Life-Cycle Safety for Composite Structures, Guangxi University, Nanning, 530003, P. R. China*
[3] *Guangxi Key Laboratory of Petrochemical Resource Processing and Process Intensification Technology, Guangxi University, Nanning, 530004, P. R. China*

Received 9 February 2023, received in revised form 8 March 2023, accepted 27 March 2023

Abstract

This study investigated the effect of Sb additions (0, 0.4, 0.8, 1.2, 1.6, and 2.0 wt.%) on the microstructure, mechanical properties, and thermal conductivity of hypereutectic Al-20Si-0.3Zr alloy. The aim was to refine and homogenize the Si phases to improve the alloy's thermal conductivity, casting fluidity, and mechanical properties. Various techniques, including SEM, EDS, XRD, DSC, a universal testing machine, and a conductivity tester, were used to analyze the as-cast specimens. The results showed that adding Sb up to 1.6 % significantly refined the morphology of primary Si, reducing its average size by 87.2 % from 376.17 to 48.30 μm, and modified the eutectic Si structure from seagrass-like to vane-like. This refinement and homogenization led to an increase in optimal elongation (El) by 183 % from 1.2 to 3.4 % and the ultimate tensile strength (UTS) by 29.4 % from 132.1 to 170.9 MPa. Furthermore, the addition of 1.6 % Sb improved the alloy's thermal conductivity and conductivity while also reducing its solidification temperature range from 442.2 to 328.5 K, improving casting fluidity. These findings suggest that Sb modification can be a useful method to improve the thermal conductivity, casting fluidity, and mechanical properties of Al-20Si-0.3Zr alloy.

K e y w o r d s: antimony, hypereutectic Al-Si-Zr alloy, modification mechanism, mechanical properties, electrical conductivity

1. Introduction

Al-Si alloys are usually used in the field of electronic packaging and automotive parts because of their low thermal expansion coefficient, wear resistance, corrosion resistance, high chemical stability, high specific strength, and castability [1–4]. A large amount of latent heat of crystallization will be released when primary silicon is precipitated from hypereutectic Al-Si alloy during solidification. Therefore, the commonly used hypereutectic Al-Si alloys have better fluidity than eutectic alloys [5].

In the field of auto parts, hypereutectic Al-Si alloys (the alloy containing more than 12.7 wt.% silicon) can be used as a substitute for cast iron for auto engine parts, such as pistons, cylinders, swing arms, and control valves, because of its low density, high specific strength, wear resistance, and low coefficient of thermal expansion, which can further reduce the weight of the car, fuel consumption, and pollution emissions [6–8].

The high thermal conductivity of hypereutectic Al-Si alloys makes them widely used in the field of electronic packaging [9]. Electrical conductivity and thermal conductivity are two fundamental physical properties of metallic materials, reflecting their performance in electron movement and heat transfer, respectively. There is a close relationship between the electrical conductivity and thermal conductivity of metals, although they may differ under specific conditions. Generally, there is a positive correlation between the electrical conductivity and thermal conductivity of metals. This is because, in metallic materials, both electrons and heat are transported through the

*Corresponding author: tel.: +8607713232200; e-mail address: tp@gxu.edu.cn

internal electron transport of metals [10]. Therefore, measuring the electrical conductivity of metals can indirectly reflect the thermal conductivity of alloys. At the same time, due to the complexity and relatively low accuracy of measuring thermal conductivity, it is a shared practice in experiments to use the measurement of electrical conductivity as a substitute for measuring thermal conductivity.

However, the application of hypereutectic Al-Si alloys is limited by its low plasticity and fracture toughness [11, 12]. The microstructure of hypereutectic Al-Si alloy is composed of a primary silicon structure and eutectic mixture (α-Al + eutectic silicon structure), where the primary silicon structure is usually in the shape of a star, polygon, plate, and sheet, while the eutectic silicon structure is in the shape of the coarse needle and sheet [13–15]. The researchers point out that the size, morphology, and distribution of the second phase in Al-Si alloy, represented by primary silicon and eutectic silicon, play a key role in mechanical properties [16, 17]. Generally speaking, the smaller the size, the more regular shape, and the more uniform the distribution of primary silicon and eutectic silicon are, the more favorable it is for the properties of the alloy [18, 19].

Zirconium is one of the earliest rare metal elements used for the microalloying of aluminum alloy [20, 21]. It can refine the microstructure of aluminum alloy, restrain nucleation and grain growth, and thus improve the strength of the aluminum alloy [22–24]. Dan Su et al. [25] studied the effect of adding Sc and Zr on the properties of AA5356 alloy and found that the grains in the fusion zone of the welded joint were significantly refined, and the properties of the alloy were improved. Zr can not only dissolve in the alloy matrix but also combine with Al to form Al_3Zr precipitates [26].

There are three forms of Al_3Zr in this alloy. First of all, it is coarse Al_3Zr, which is unfavorable to the alloy properties. The second kind is metastable Al_3Zr, which can improve the properties of the alloy because of the coherent structure of precipitates and the matrix. The third is the stable Al_3Zr equilibrium precipitate, which is not coherent with the matrix and has an adverse effect on the performance of the alloy. Studies have shown that when the Zr addition is 0.3 %, the Al-20Si alloy has better performance, and Al_3Zr precipitates formed when Zr addition exceeds 0.3 % will deteriorate the performance of aluminum alloys [27-29].

Adding trace elements to hypereutectic Al-Si alloys to control the shape and size of the second-phase particles and ultimately improve the performance of the alloy is an effective method in industrial production [30]. The silicon morphology of Al-Si alloys can be effectively changed into a fibrous structure after modification treatment.

Na, Sb, and Sr are common modifiers in the aluminum industry [31–33]. The sodium-containing modifier is one of the most shared modifiers with perfect modification, early application, and outstanding effects in the conventional process of the aluminum industry [34]. However, the modification of the sodium-containing modifier usually weakens after 30–60 min, and the sodium-containing modifier has a corrosive effect on the crucible and will become invalid after remelting [35]. The modification effect of a strontium-containing modifier is similar to that of a sodium-containing modifier, and the effect is more lasting. But Sr can improve the hydrogen absorption capacity of the melt and easily lead to pinholes, shrinkage porosity, and other defects in aluminum alloys.

The antimony-containing modifier not only has no such problems but also can refine the eutectic silicon crystals of Al-Si alloy [36]. Quite a few studies manifest that during the solidification process of aluminum alloy, Sb and molten aluminum form AlSb particles together; these AlSb particles act as heterogeneous nucleating agents of eutectic silicon crystals, resulting in the formation of finely layered morphology of eutectic silicon crystals [37]. Yang et al. [38] pointed out that Sb can refine and spheroid the eutectic silicon structure of A357 aluminum alloy, thereby improving wear and tensile properties.

Previous studies have shown that antimony can accelerate the formation kinetics of the Zr-rich precipitate shell in the aluminum alloy, and there is an attraction between Zr and Sb; Sb may enhance the diffusion of Zr in aluminum alloy [39]. Up to now, there has been no report on the influence of different Sb additions on the microstructure and properties of hypereutectic Al-Si alloy with 0.3 % Zr content. The study of Cleiton Luiz Pereira et al. [40] demonstrates that the tensile properties of Al-15Si alloy with 1 % Sb can be improved. The optimum addition amount of Sb in Al-20Si-0.3Zr is not clear. On this basis, six groups of Al-20Si-0.3Zr-xSb (x = 0, 0.4, 0.8, 1.2, 1.6, 2.0) alloys were prepared by the permanent mold casting method. The hypereutectic Al-Si-Zr-Sb alloy with the best comprehensive properties was expected to obtain by observing the microstructure of the alloy, counting the size of the precipitates, analyzing the composition of various parts of the alloy, and testing the properties of the alloy.

2. Materials and methods

The raw materials of the prepared alloys used in the current study were supplied by Sichuan Land High-tech Industry Co., Ltd. The Al-20Si-0.3Zr-xSb alloys (x = 0.4, 0.8, 1.2, 1.6, 2.0) were prepared in an SG2-7.5-10 energy-saving resistance furnace. Raw material composition is shown in Table 1. The corresponding chemical compositions of these alloys used in

Table 1. Chemical composition of the materials used in this work

Raw materials	Chemical composition (wt.%)						
	Si	Zr	Sb	Mn	Fe	Impurity	Al
Al-20Si	19.98	–	–	0.11	0.08	No more than 0.08	Bal.
Al-10Zr	–	9.72	–	–	0.03	No more than 0.07	Bal.
Al-5Sb	–	–	4.98	–	0.02	No more than 0.03	Bal.
Pure Al	–	–	–	–	–	No more than 0.30	Bal.

Table 2. Summary of the experimental alloys with different Sb addition (wt.%)

Samples number	Modifier dosage	Chemical composition of the experimental alloys						
		Si	Zr	Sb	Mn	Fe	Impurity	Al
1	0	20.0	0.3	–	0.11	0.08	No more than 0.2	Bal.
2	0.4	19.86	0.27	0.39	0.09	0.09	No more than 0.2	Bal.
3	0.8	19.78	0.29	0.76	0.08	0.12	No more than 0.2	Bal.
4	1.2	19.56	0.30	1.12	0.11	0.11	No more than 0.2	Bal.
5	1.6	19.37	0.28	1.52	0.07	0.10	No more than 0.2	Bal.
6	2.0	19.12	0.32	1.88	0.06	0.09	No more than 0.2	Bal.

the current study were measured by a direct-reading spectrometer (SPECTROLAB/M11, Germany).

Firstly, Al-20Si alloy was melted at 1013 K and kept for 10–15 min. Then the Al-5Sb and Al-10Zr master alloys preheated to 473 K were added to the Al-Si alloy melt, and the molten aluminum alloy was uniformly stirred for about 2 min. After the raw material is fully reacted, the molten aluminum alloy is cooled to 993 K and stood for 3–5 min. Finally, an appropriate amount of C_2Cl_6 is added to the molten aluminum for refining and degassing. After deslagging, the refined alloy liquid is then stood for 10–15 min. The molten aluminum is poured into a cylindrical steel mold preheated to 473 K to obtain Al-20Si-0.3Zr-xSb alloys with various nominal compositions. The composition of the alloy samples obtained by the experiment is listed in Table 2.

The metallographic sample is cut off evenly at 15 mm from the bottom of the metal mold and then polished to a mirror state with sandpaper and polishing equipment step by step. The metallographic specimens were observed under an optical microscope after etching with Keller's reagent for 30 s. Then, the metallographic samples were subjected to a deep corrosion test. The metallographic sample was deeply etched in 15 % NaOH solution in a 333 K water bath for 15 min to characterize the three-dimensional morphology of Si phases, then washed with concentrated nitric acid and distilled water in turn, and then dried.

The tensile properties were tested by Instron 8801 electronic universal testing machine. The standard distance of samples was D 55 mm × 5 mm × 2.5 mm, and the tensile speed was 1 mm min^{-1}. Five tensile samples were prepared for each sample, and the average value was calculated. In addition, a Philips X'Pert MPD Pro X-ray diffractometer was used for phase analysis, and Hitachi TM4000 Plus desktop scanning electron microscopy (SEM) was used to observe the high-power microstructure of the alloy. EDS was used to analyze the distribution of elements in the precipitated phase. The surface morphology of tensile fracture was observed by SEM, and EDS element detection was performed on typical fracture morphology to analyze its fracture mechanism. Meanwhile, the metamorphism mechanism of Zr and Sb elements in the second phase of Al-20Si alloy was analyzed by EDS.

The electrical conductivity of the alloy samples was measured by a Sigma 2008 digital eddy current metal conductivity meter. Each aluminum alloy sample was tested five times, and the average of the results was taken as the final electrical conductivity of the alloy. In order to clarify whether there is a phase transition in Al-20Si alloy after Zr and Sb compound modification, DSC analysis was carried out on the alloy. The sample was cut 20–30 mg alloy particles for ultrasonic cleaning, drying alloy particles after the test; the heating rate was selected for 283 K min^{-1}, and the test temperature range was selected for room temperature (298 K) to 1073 K. The experiment used STA 449 F3 Jupiter synchronous thermal analyzer produced by NETZSCH company in Germany for DSC analysis.

3. Results

3.1. Effect of Sb on the microstructure of Al-Si-Zr-Sb alloys

Figure 1 shows the optical microstructure of the cast hypereutectic Al-Si-Zr-Sb alloy. Three main types

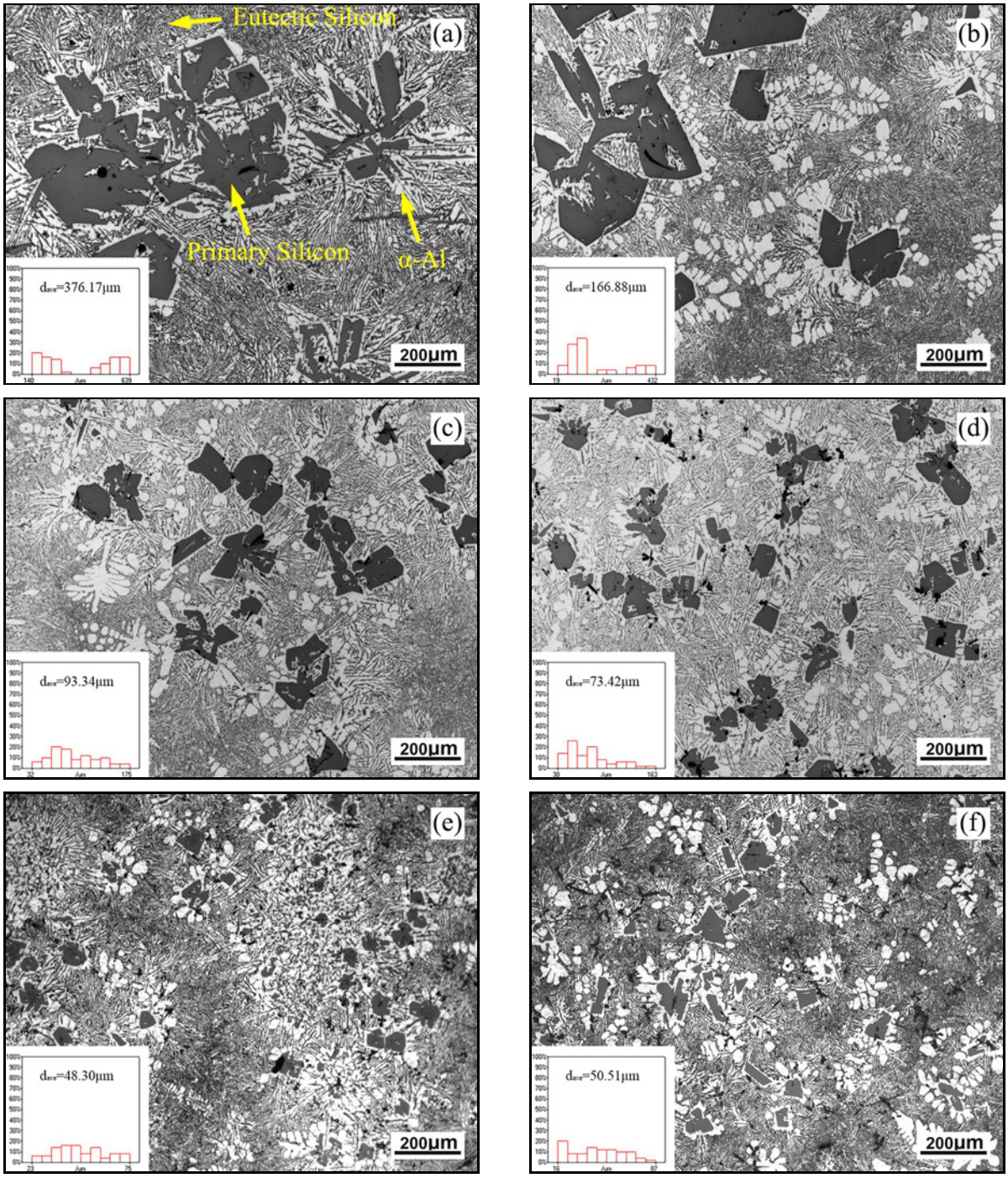

Fig. 1. Optical micrographs of the Al-20Si-0.3Zr alloys with various content of Sb: (a) unmodified, (b) 0.4 % Sb, (c) 0.8 % Sb, (d) 1.2 % Sb, (e) 1.6 % Sb, and (f) 2.0 % Sb.

of crystals were observed: the first type is the silver-white α-Al phase, the second type is the primary silicon phase that appears as black polygons, and the third type is the eutectic silicon phase that appears as black-white interdendritic lamellae. In this study, 50 primary silicon particles were selected at different locations to quantitatively measure the grain size of primary Si crystals, as indicated in the lower left corner of each image in Fig. 1.

From Fig. 1a, it can be seen that the primary silicon phase in the Al-20Si-0.3Zr alloy mainly appears as fragmented plates, with an average grain size of up to 376.17 μm. Figures 1b,c,d show the morphology of the primary silicon phase in hypereutectic Al-Si-Zr--Sb alloys containing 0.4, 0.8, and 1.2 % Sb, respectively. After the addition of Sb to the Al-20Si-0.3Zr alloy, most of the primary silicon phases become smaller and rounder. As the Sb content increases, the shape

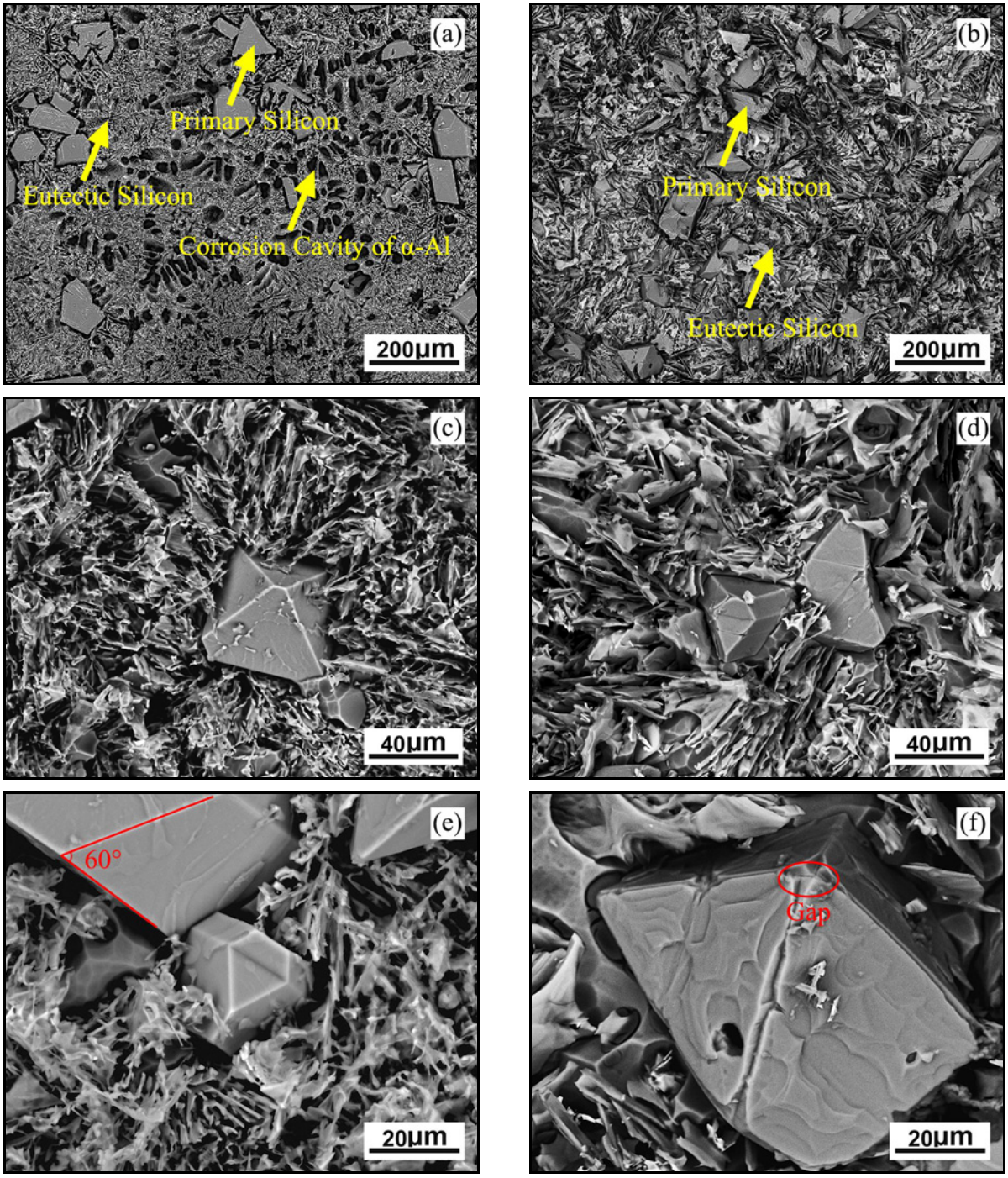

Fig. 2. The 3D morphology of primary Si: (a), (c), and (e) base alloys; (b), (d), and (f) medicated Al-Si-Zr-Sb alloy.

of the primary silicon phase in the alloy becomes more regular, and the distribution becomes more uniform. The average grain size gradually decreases to 166.88, 93.34, and 73.42 μm, respectively. When 1.6 % Sb is added to the Al-20Si-0.3Zr alloy (Fig. 1e), the grain size of the primary silicon phase decreases from the unmodified size of 376.17 to 48.30 μm, a reduction of 87.2 %. However, when the Sb addition amount is increased to 2.0 %, the size of the primary silicon phase begins to increase, and some of the primary silicon phases exhibit irregular shapes. Figure 1f shows that the grain size of the primary silicon phase increases to 50.51 μm, indicating that 2.0 % Sb is not conducive to the refinement of the primary silicon phase.

Figure 2 shows the three-dimensional morphology of the hypereutectic Al-Si-Zr-Sb alloy. It can be observed that the primary silicon phase of the Al-20Si-0.3Zr alloy (Fig. 2a) exhibits a polyhedral and diamond-like shape, and the eutectic silicon phase has a fine and uniform morphology. The pores left after the

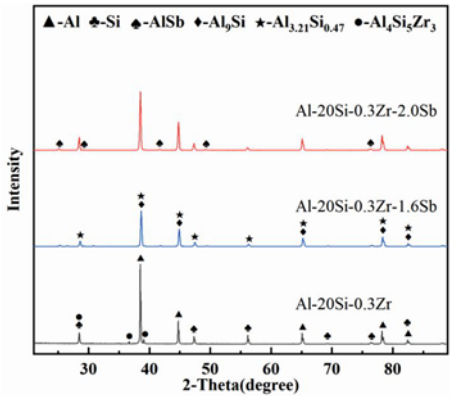

Fig. 3. The XRD patterns of the Al-20Si-0.3Zr alloy with various content of Sb.

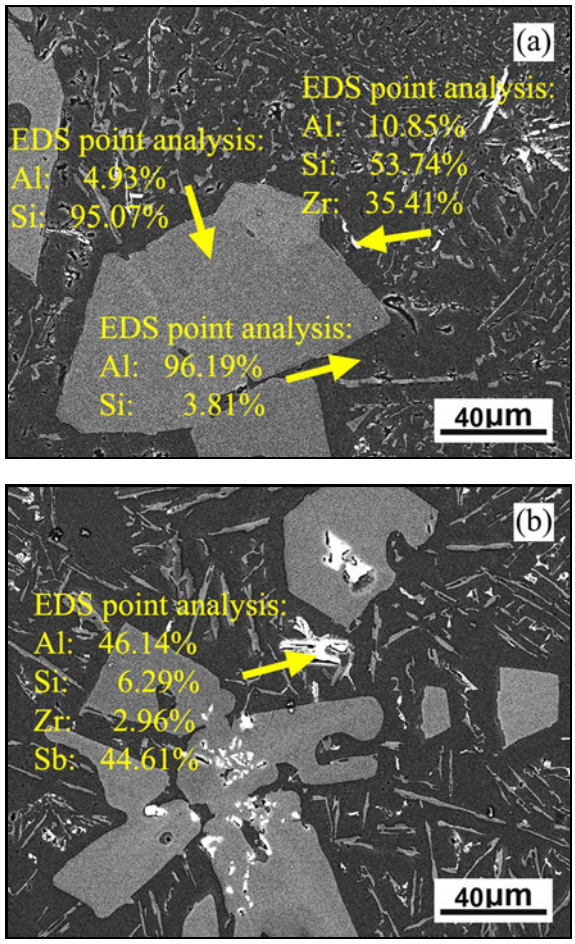

Fig. 4. SEM and EDS analysis of the second phase: (a) base alloy and (b) Al-20Si-0.3Zr-1.6Sb.

corrosion of α-Al in the alloy can be clearly observed. The primary silicon morphology of the hypereutectic Al-Si-Zr-Sb alloy with Sb addition (Fig. 2b) is irregular and gravel-like, and the regularity is reduced. The eutectic silicon phase grows into a shape resembling paper scraps, with the primary silicon more tightly embedded within it. Additionally, the corrosion pits of α-Al disappear in the alloy. Figures 2c,d show that the eutectic silicon morphology of the Al-20Si-0.3Zr alloy (Fig. 2c) is small and seaweed-like, with a large gap between the eutectic silicon phase and primary silicon phase and a small contact area. The eutectic silicon morphology of the hypereutectic Al-Si-Zr-Sb alloy with Sb addition (Fig. 2d) becomes larger and blade-like, with the eutectic silicon phase tightly combined with the primary silicon and a relatively large contact area. From Figs. 2e,f, it can be observed that the primary silicon phase of the Al-20Si-0.3Zr alloy (Fig. 2e) has a smooth and regular polyhedral shape with angles of 60° between the edges. The eutectic silicon phase exhibits a dendritic shape, with primary and secondary branches contacting the primary silicon phase as points. The primary silicon edges of the hypereutectic Al-Si-Zr-Sb alloy with Sb addition (Fig. 2f) are defective and rough, presenting an irregular shape. The eutectic silicon phase is layered and in contact with the primary silicon surface.

Figure 3 presents the XRD patterns of the Al-20Si-0.3Zr alloy before and after Sb addition. The XRD pattern shows that, in addition to the inherent Al and Si phases, several secondary phases, including $Al_4Si_5Zr_3$, Al_9Si, and $Al_{3.21}Si_{0.47}$, are observed in the Al-20Si-0.3Zr alloy. However, the addition of Sb leads to the appearance of a new phase, AlSb, in the alloy. This result indicates that Sb addition promotes the formation of the AlSb phase, which may improve the mechanical and physical properties of the Al-20Si-0.3Zr alloy.

Figure 4 shows the SEM images and EDS point scanning results of Al-Si-Zr-Sb alloys with different Sb contents. Two types of silver-white precipitates were found in the alloys. When Sb was not added, there were three components in the second phase, namely aluminum, silicon, and zirconium. Combined with the results of X-ray diffraction analysis, the silver-white second phase in the alloy was identified as $Al_4Si_5Zr_3$. After adding Sb to the alloy, Sb was found in the silver-white second phase, indicating that a certain AlSiSbZr second phase may appear in the alloy. In the EDS results of Fig. 4b, the atomic ratio of Al to Sb was concerning 1:1, accordingly, so it was confirmed that AlSb was present in the second phase, but the silver-white second phase may also be composed of multiple precipitates. In the Al-20Si-0.3Zr alloy without Sb, the morphology of the eutectic silicon phase was short rod-shaped and spiral-shaped. After adding Sb to the alloy, the eutectic silicon phase became needle-shaped, which was more similar to the Al-20Si alloy without Zr. It can be seen that Sb can offset some of the metamorphic effects of Zr on the eutectic silicon of Al-20Si alloy.

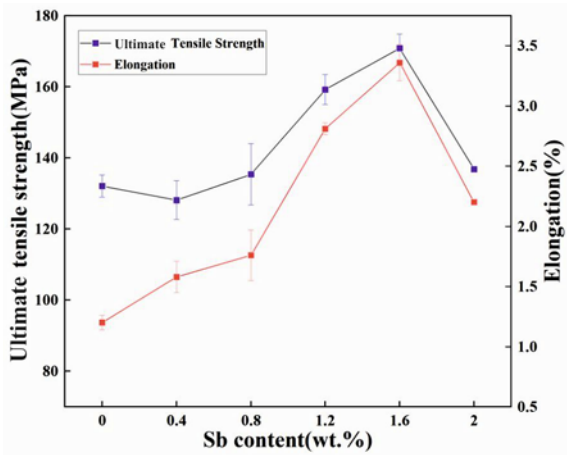

Fig. 5. Mechanical properties of Al-20Si-0.3Zr alloys with various content of Sb.

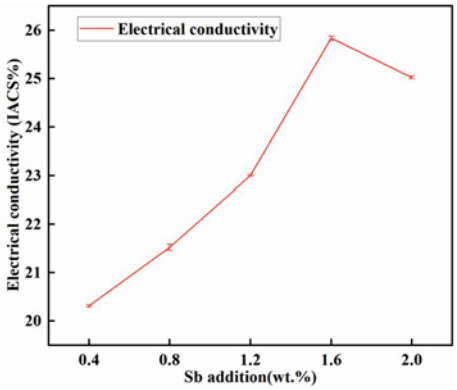

Fig. 6. Electrical conductivity of Al-20Si-0.3Zr alloys with various content of Sb.

3.2. *Effect of Sb on properties of Al-Si-Zr-Sb alloy*

Figure 5 is the histogram of the ultimate tensile strength (UTS) and elongation (El) of hypereutectic Al-20Si-0.3Zr alloy with different contents of Sb. Obviously, with the increase of Sb content, both the tensile strength and elongation of aluminum alloy are improved. When the addition of Sb increased to 1.6 %, the ultimate tensile strength increased from 132.1 to 170.9 MPa, an increase of 29.4 %. The elongation increased from 1.2 to 3.4 %, an increase of 183 %. How-

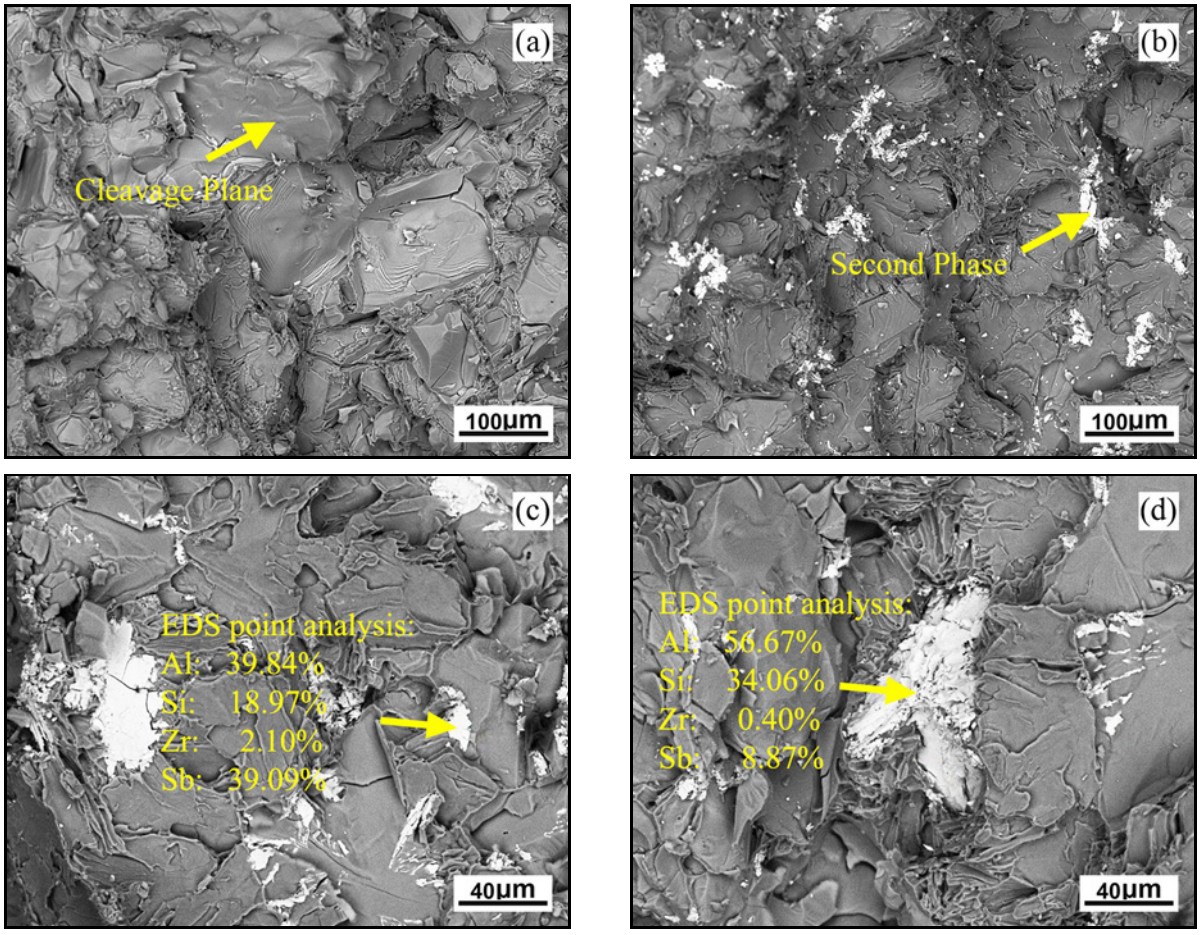

Fig. 7. Fracture morphology of the Al-20Si-0.3Zr alloy with various content of Sb: (a) base alloy, (b) Al-20Si-0.3Zr-0.8Sb, (c) Al-20Si-0.3Zr-1.6Sb, and (d) Al-20Si-0.3Zr-2.0Sb.

ever, when the addition of Sb is less than 0.8 %, the ultimate tensile strength of Al-20Si-0.3Zr alloy has little change.

Figure 6 is the conductivity of Al-20Si-0.3Zr alloy with the different contents of Sb. The experimental results show that with the increase of Sb content from 0.4 to 2 %, the electrical conductivity of Al-20Si-0.3Zr alloy first increases and then decreases, and the electrical conductivity reaches the maximum value when the Sb content is 1.6 %, 25.8 IACS %.

Figure 7 shows the tensile fracture morphology and EDS point analysis of hypereutectic Al-Si-Zr-Sb alloys with different Sb contents. As shown in Fig. 7a, a large area of cleavage surfaces and local radial river patterns can be observed on the tensile fracture surface of the Al-20Si-0.3Zr alloy. Due to the larger size of the primary silicon phase on the alloy matrix, the primary silicon phase itself can fracture, and the junction between the primary silicon and the matrix can also serve as a source of fracture. Figure 7b shows the tensile fracture morphology of the Al-20Si-0.3Zr alloy with added Sb. It can be observed from the figure that a significant white second-phase precipitation is formed in the alloy after Sb addition. In addition, the large smooth cleavage surfaces are no longer visible, and the river-like patterns increase. To determine the composition of the second phase formed by adding Sb, an EDS analysis of the second phase was performed. Figures 7c,d show the EDS point analysis of the fracture of the alloy after adding Sb. It can be seen from the figures that the silver-white second phase precipitate contains four elements: Al, Si, Zr, and Sb.

Figure 8 shows the differential thermal analysis data of hypereutectic Al-Si-Zr-Sb alloys. The data show that when the additional amount of Sb is 1.6 %, the peak value of the endothermic peak is the largest, reaching 875.9 K, and the onset temperature and endpoint temperature of the enthalpy change is the smallest, 845.5 and 901.0 K, respectively. When the additional amount of Sb is 1.6 %, there is no protrusion on the endothermic peak of the hypereutectic Al-Si-Zr-Sb alloy.

Figure 9 shows the solidification temperature range of the Al-20Si-0.3Zr alloy with different Sb concentrations. It can be found that with the increase of Sb content, the solidification range of the alloy decreases first and then increases. When the content of Sb is 1.6 %, the range of solidification temperature is the smallest, which is 328.5 K.

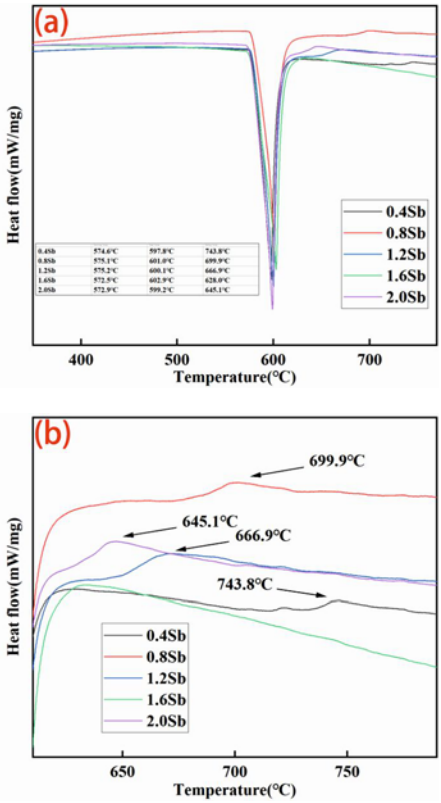

Fig. 8. DSC curve of Al-20Si-0.3Zr alloys with various content of Sb.

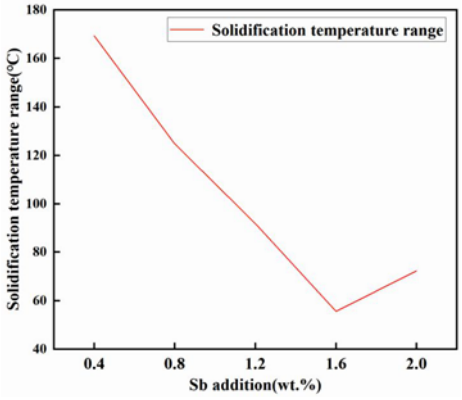

Fig. 9. Solidification temperature range of Al-20Si-0.3Zr alloys with various content of Sb.

4. Discussion

4.1. Modification mechanism

In this study, the main alloying element in the alloy is Si. Due to its low solid solubility in aluminum, the maximal equilibrium solubility of silicon in aluminum is limited to 1.6 % by weight [41]. The Si element is typically present in the form of primary silicon, eutectic silicon, and Si-containing precipitates in the alloy. Coarse silicon in the Al-Si alloy can trigger severe damage to the mechanical properties and processability of the alloy by weakening the aluminum matrix. As a result, the material's plasticity, toughness, and strength are significantly reduced.

Reza Haghayeghi et al. demonstrated that antimony (Sb) refines the primary silicon (Si) crystal via twinning and increasing stacking fault density through the Impurity-Induced Twinning (IIT) mechanism [42]. Experimental results indicate that the refinement of primary silicon in Al-20Si-0.3Zr alloy is most effective when the Sb content is approximately 1.6 %. The theory of IIT was proposed by Lu and Hellawell [43] following extensive experimental investigations. It is believed that the ratio of the modifier atomic radius to Si atomic radius is the decisive factor in measuring the modification effect, and when the ratio of the modifier atomic radius to Si atomic radius is equal to or close to 1.646, this modifier will possess an excellent modification effect. The ratio of the atomic radius of Sb (0.153 nm) to the atomic radius of Si (0.117 nm) is 1.31, which has a certain effect. Therefore, during the solidification process, Sb atoms are adsorbed to the steps or twin grooves of the Si phase growth interface, sealing the original atomic steps and twin grooves, forcing the Si phase to change its growth morphology.

At the same time, there is a large atomic radius difference between Sb and Si. Sb atoms embedded in the lattice of Si will induce high-density atomic steps and twin grooves. The steps and twin grooves that appear will cause the disappearance of steps and twin grooves because of the adsorption of active Sb atoms, which will lead to the continuous change of the growth direction of the Si crystal and modify the primary Si crystal. In this study, it is found that the Sb-containing compounds generated exist in the interior of the primary Si crystal (Fig. 4), which will play the role of heterogeneous nucleation, thus effectively refining the primary Si crystal structure. On the other hand, according to the ternary phase diagram, the solubility of Sb in Al and Si is intensely limited. During the solidification process, with the decrease of the alloy melt temperature, Sb is pushed into the liquid phase at the front of the Si interface. And the concentration of solute leads to the increase of the undercooling at the front of the interface, which inhibits the growth of the Si phase and refines the structure of the Si phase. Therefore, the modification mechanism of element Sb on the Si phase in Al-Si alloy can be summarized as follows: (1) impurity-induced twinning mechanism, (2) heterogeneous nucleation mechanism, and (3) crystal growth inhibition mechanism.

O. Uzun et al. investigated the modification effect and mechanism of the Sb element on eutectic silicon in Al-12Si alloy. They found that the optimal structure of the alloy was achieved with an Sb content of 0.5 %, and the eutectic structure did not further refine but instead coarsened when the Sb content continued to increase to 1.0 %. Analysis showed that when the Sb content in the alloy reached a certain mass fraction, the formation of the AlSb compound during the solidification process of the alloy would result in the segregation of the Si phase. In this experiment, the optimal Sb addition amount for Al-20Si-0.3Zr alloy was found to be 1.6 %, indicating that the optimal Sb content may vary with changes in the matrix alloy composition, which requires further experimental verification [44].

Furthermore, this study characterized not only the planar eutectic silicon structure of the hypereutectic Al-Si alloy but also the three-dimensional structure of the eutectic silicon. The results showed that the addition of Sb transformed the three-dimensional seaweed-like structure of eutectic silicon in the Al-20Si-0.3Zr alloy into a three-dimensional layered structure.

4.2. Strengthening mechanism

The fracture of Al-20Si-0.3Zr alloy is caused by a sea of factors, including primary silicon, eutectic silicon, and the morphology of the second phase. According to the literature [45], the main factors affecting the fracture of Al-Si alloy can be summarized as follows: (1) The difficulty of Si phase crack generation, (2) The bonding strength between Si phase particles and metal matrix. During the tensile process, the tensile stress acting on the Si-phase particles gradually increases. When the tensile stress acting on the Si-phase particles exceeds the maximum tensile stress that it can bear, the Si-phase particles will fracture, accompanied by the generation and expansion of new cracks. When these cracks are connected with each other and penetrate the specimen section, the specimen fracture will occur. The maximum stress that nascent Si can bear is shown in Eq. (1):

$$\sigma_{\mathrm{f}} = \left(\frac{2E\gamma}{\pi C}\right)^{\frac{1}{2}}, \tag{1}$$

where γ is the surface fracture energy, E is the elastic modulus, and C is the defect length inside the grain. From the microstructure diagram, it can be seen that the defect length inside the coarse primary Si is significantly longer than the defect length after modification, thus reducing the maximum tensile stress. On the other hand, the stress concentration of coarse primary crystalline silicon and the needle-like eutectic silicon is caused by the existence of tips. Therefore, under the same external force, the unmodified coarse Si phase is more likely to fracture.

Other researchers [46] have proposed the mechanical conditions for the second phase to break away from the matrix interface and produce cracks when plastic deformation occurs around the second phase particles in the alloy:

$$\sigma = \frac{1}{k}\left(\frac{E\gamma}{d}\right)^{\frac{1}{2}} + \frac{\sigma_{\mathrm{s}}}{k}\left(\frac{\Delta V}{V}\right)^{\frac{1}{2}}, \tag{2}$$

where σ is the tensile stress when the interface is detached, k is the stress concentration factor at the particle, γ is the surface fracture energy, E is the weighted average of the elastic modulus of particles and matrix, σ_s is the yield strength of the matrix, ΔV is the deformation volume of the matrix around the particles, and V is the volume of the second phase particles. It can be seen from Eq. (2) that the smaller the size of Si particles and other second phases, the greater the stress required for Si particles and other second phases to separate from the matrix, and the greater the tensile strength of the alloy. At the same time, the more significant the stress concentration in the alloy, the greater the stress concentration factor k value, the smaller the stress of interface separation, and the smaller the tensile strength. Therefore, from Eq. (2), it can be seen that the tensile strength of hypereutectic Al-20Si-0.3Zr alloy can be improved by controlling the morphology of the Si phase and other second phases, reducing their size, improving their morphology, achieving the purpose of reducing their size and edge passivation.

In this study, with the increase of Sb content in the Al-Si-Zr-Sb alloy, it was found that the reduction of primary silicon size could lower the probability of extensive cleavage fracture in the alloy. The reduction in the individual size of primary silicon could decrease the probability of transgranular fracture and increase the difficulty of intergranular fracture in the alloy. Moreover, the passivation of the primary silicon edge could decrease the stress concentration in the alloy and reduce the possibility of crack initiation and propagation. On the other hand, the coarsening of eutectic silicon, including both the 2D needle-like and 3D sheet-like structures, could increase the number of crack sources and provide channels for crack propagation, which would negatively affect the mechanical properties of the alloy. Additionally, the increase of the second-phase precipitation in the alloy could lead to stress concentration and further impair the mechanical properties of the alloy.

Elemental ratio analysis based on EDS and XRD results suggests that the silver-white second phase in the alloy may contain AlSb precipitation, a well-known phenomenon. In previous studies on the influence of Sb on Al-Si alloys, the optimal Sb content in Al-Si alloys was generally less than 1.6 %. This indicates that the increase in optimal Sb content in Al-Si-Zr-Sb alloys may be attributed to the influence of Zr on Sb. Furthermore, the EDS analysis result in this study showed that there might be $ZrSb_2$ ($Zr + Sb \rightarrow ZrSb_2$) and $ZrSi_{0.7}Sb_{1.3}$($Zr + Si + Sb \rightarrow ZrSi_{0.7}Sb_{1.3}$) in the silver-white second phase, which can contribute to the increase of the optimal Sb content in the Al-Si-Zr-Sb alloy. For Al-20Si-0.3Zr alloy, the optimal Sb addition amount is 1.6 %. When the Sb content in the alloy exceeds 1.6 %, the size of the silver-white second phase will continue to increase, becoming one of the sources of fracture and deteriorating the mechanical properties of the alloy. It is suggested that different Zr contents may affect the optimal Sb content for the Al-Si-Zr-Sb alloy.

When the amount of Sb added to Al-20Si-0.3Zr alloy is not more than 0.8 %, the tensile strength of the alloy does not significantly improve and even decreases, which is different from Sb added to Al-20Si alloy without Zr. Studies have shown that when Sb is added in trace amounts to Al-20Si alloy, the tensile strength of the alloy monotonically increases as the Sb content increases. There are two possible reasons for this phenomenon: the first possibility is that a small amount of Sb can lead to the refinement of primary silicon phases, the blunting of primary silicon phase edges, the coarsening of eutectic silicon phases, and the formation of a second phase containing AlSb in the alloy. However, at this time, the decrease in mechanical properties of Al-Si alloys caused by the coarsening of eutectic silicon phases and the increase in the second phase is equal to or slightly greater than the improvement in mechanical properties caused by the refinement of primary silicon and the blunting of primary silicon edges, resulting in little change or even a slight decrease in the mechanical properties of the alloy. The second possibility is that due to the presence of Zr in the alloy, Sb is first attracted or forms a second phase by Zr after being added to the alloy. The actual amount of Sb that produces a modification effect is smaller than the amount added, and the negative impact caused by the formation of a second phase is greater than the positive impact of Sb modification, resulting in a small decrease in the tensile strength of the alloy. This requires further improvement of testing methods to explore.

As the Sb content increases continuously and does not exceed 1.6 %, the improvement in the mechanical properties of the aluminum alloy due to the refinement and blunting of primary silicon is greater than the decrease in the mechanical properties of the aluminum alloy due to the coarsening of eutectic silicon and the increase in the second phase. Therefore, the comprehensive performance of the alloy shows an improvement.

When the Sb content exceeds 1.6 %, the refinement and blunting of primary silicon will slow down. When the improvement in the mechanical properties of the aluminum alloy due to the refinement and blunting of primary silicon is less than the decrease in the mechanical properties of the aluminum alloy due to the coarsening of eutectic silicon and the increase in the second phase, the mechanical properties of the aluminum alloy will begin to deteriorate (Fig. 10).

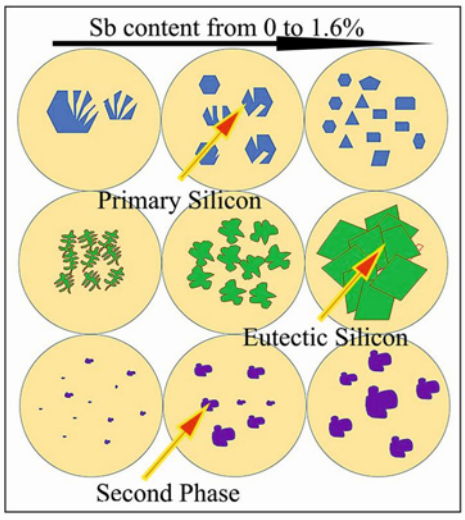

Fig. 10. Structure change mechanism diagram of aluminum alloy.

4.3. Electrical performance analysis

According to the theory of modern quantum mechanics, resistance is when electrons are hindered by lattice nodes when they propagate in the form of waves under the action of an electric field [47]. When the lattice is no longer regular, and the arrangement is no longer neat, the resistance will increase. According to the theory of metal conductivity, the higher the integrity of the metal crystal, the fewer crystal defects and the smaller the resistance. There are a host of factors affecting the conductivity of metal conductors.

The temperature has an impact on the conductivity of metals [48]. Generally speaking, the increase in temperature will increase the disorder of metal atoms, coupled with the intensification of thermal vibration; these changes will increase the possibility of the dispersion of electrons in the metal, thus increasing the resistance of the metal.

Plastic deformation has an impact on the conductivity of metal [49]. First, plastic deformation will distort the crystal network of metal. Secondly, plastic deformation will increase the number of crystal defects. These two factors will make the electric field near the crystal lattice extremely uneven so that the resistance of the metal will rise.

Effect of stress on metal conductivity [50]. As an example, during the use of cables, tensile stress is inevitable, and tensile stress will increase the metal resistance. The reason is that tensile stress can easily make the atomic spacing larger so that the lattice will deform, and the resistance will increase, while compressive stress is the opposite, and compressive stress can reduce the resistivity.

Chemical composition is invariably the most crucial factor [51]. The more impurities in aluminum alloy, the higher the resistivity, and when the impurities reach a certain level, the material cannot be used as a conductor. Generally speaking, when any alloy becomes a solid solution, whether the metal with relatively low resistivity dissolves into the metal with high resistivity or the metal with high resistivity dissolves into the metal with low resistivity, the conductivity will decrease. The reason for this is divided into several aspects: first of all, when the crystal lattice is distorted, the scattering probability of electrons will increase. Secondly, it is also related to the chemical action of different elements: different kinds of atoms will destroy the lattice, accordingly, the resistivity of metals will increase. In addition, the ordered change of the solid solution of the metal will strengthen the interaction between the various components so that the number of conductive electrons will be reduced. There is a main role and a secondary role in this, consequently, the resistivity decreases under the synergistic effect.

A slice of literature shows that the existing form of the silicon phase has an obvious effect on the conductivity of Al-Si alloy [52]. For example, the existence of coarse lamellar and acicular eutectic silicon in the aluminum alloy will hinder the transmission of electrons to a certain extent. Naturally, the resistance of aluminum alloy will increase at this time. When the coarse lamellar and acicular silicon is modified and changed into fibrous silicon, the resistance can be reduced. For the solid solution silicon in the alloy matrix, due to the natural difference in the lattice constants of aluminum and silicon, the solid solution silicon will lead to lattice distortion, make the crystal regularity lower, and thus increase the resistance [53].

In this study, the modification of Al-20Si-0.3Zr alloy by Sb will transform seaweed fibrous eutectic silicon into coarse lamellar eutectic silicon, but the electrical conductivity of the alloy shows an upward trend. Based on this, it is inferred that there are two possibilities. One is that the adverse effect of the morphology change of eutectic silicon on the electrical conductivity of the alloy is a secondary factor, while the modification of Sb plays a leading role in improving the electrical conductivity of Al-20Si-0.3Zr alloy. Another possibility is that the morphology change of eutectic silicon can improve the conductivity of the alloy.

4.4. Thermomechanical analysis

The essence of heat conduction of materials is that the uneven distribution of temperature leads to the transfer of heat energy from the high-temperature area to the low-temperature area [54]. The main carrier of metal heat transfer is free electrons, and free electrons play a leading role.

In metals, lattice vibration, that is, phonon heat

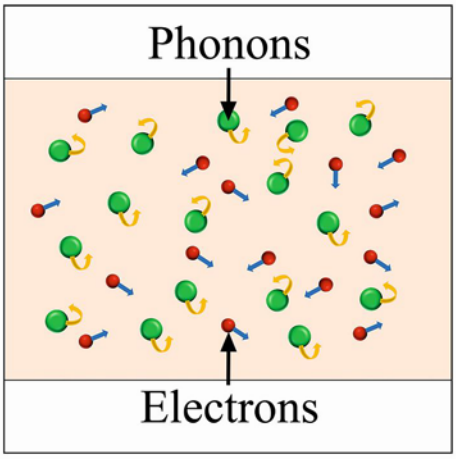

Fig. 11. Electron and phonon motion models in metal crystal materials.

conduction, also plays a role in the heat conduction process, accordingly the thermal conductivity of metals (Fig. 11) is mainly composed of electronic thermal conductivity (λ_e) and phonon thermal conductivity (λ_L), among them, the electron thermal conductivity is dominant [55]. Eq. (3) is expressed as:

$$\lambda = \lambda_e + \lambda_L. \tag{3}$$

According to Weidman-Franz law:

$$L_0 = \frac{\lambda}{\sigma T} = \frac{\pi^2}{3}\frac{k_B^2}{e^2}, \tag{4}$$

$$L_0 = 2.45 \times 10^{-8}\ \mathrm{W}\frac{\Omega}{\mathrm{K}^2} \tag{5}$$

where L_0 is Lorentz constant, k_B is Boltzmann constant ($\mathrm{J\,K^{-1}}$), T is the absolute temperature, e is electronic power, and σ is the conductivity of the metal. The ratio of the thermal conductivity to the electrical conductivity of a metal is constant at room temperature and does not vary from metal to metal [56]. Therefore, it can be inferred that the thermal conductivity of Al-20Si-0.3Zr alloy will increase at first and then decrease with the increase of Sb addition before and after Sb modification. When the content of Sb is 1.6 %, the thermal conductivity of Al-20Si-0.3Zr alloy is the highest.

The DSC method is a paramount means to analyze the phase transition temperature and latent heat of the material. It has been widely used in the analysis of the phase transition process of the alloy. When the alloy temperature rises to a certain extent, the bonding between the molecules in the metal will break, resulting in a change of the phase structure, thus forming an absorption peak on the DSC curve [57]. As is known to all, the smaller the solidification temperature range of aluminum alloy, the better the casting fluidity of aluminum alloy. Therefore, it can be seen from the results shown in Fig. 9 that the casting fluidity of Al-20Si-0.3Zr alloy first increases and then decreases with the increase of Sb content. When the content of Sb is 1.6 %, the alloy has the strongest fluidity. In other words, the addition of Sb in Al-20Si-0.3Zr alloy can improve the fluidity of the alloy.

By observing the differential thermal analysis curve of the alloy, it can be found that with the increase of Sb addition in the alloy, the end temperature of the endothermic peak of enthalpy change of the alloy gradually decreases. When the addition of Sb exceeds 1.6 %, the endpoint temperature begins to rise, and its changing trend is consistent with the electrical conductivity and mechanical properties after the fracture of the alloy. As the end temperature of the endothermic peak of the enthalpy change of the alloy is related to the second phase in the alloy, it can be seen that the second phase of the Al-Si-Zr-Sb alloy has a dominant influence on the electrical conductivity, thermal conductivity, and mechanical properties.

5. Conclusions

The incorporation of Sb into the hypereutectic Al-20Si-0.3Zr alloy resulted in a transformation of the primary silicon phase morphology from coarse, irregularly shaped broken plates to fine granular blocks, with an 87.2 % decrease in average size from 376.17 to 48.30 μm. As the Sb content increased, the morphology of the eutectic silicon phase transformed from seaweed-like to leaf-like.

The mechanical properties of the Al-20Si-0.3Zr alloy were significantly improved with the addition of Sb, resulting in a 29.4 % increase in ultimate tensile strength from 132.1 MPa to 170.9 MPa and a 183 % increase in elongation from 1.2 to 3.4 % at 1.6 % Sb content. The Sb modification also improved thermal and electrical conductivity and reduced the solidification temperature range from 442.2 to 328.5 K, thereby enhancing the casting fluidity of the alloy.

The optimal Sb addition in Al-20Si alloy with 0.3 % Zr was 1.6 %. Further investigations are needed to explore the effect of higher Sb content and varying Zr content on the properties of hypereutectic Al-Si alloys.

Acknowledgements

This research was supported by the National Natural Science Foundation of China (52261024), the China Postdoctoral Science Foundation Funded (2021M693800), and the Opening Project of Guangxi Key Laboratory of Petrochemical Resource Processing and Process Intensification Technology (2022K005).

References

[1] P. Tang, Q. Liu, F. Yu, F. Mo, L. Qin, Effect and its mechanism of fixed-ratio and incremented 3Be-Sb complex modifier on microstructures and properties of hypereutectic Al-Si-Mg alloy, Journal of Alloys and Compounds 931 (2023) 167478. https://doi.org/10.1016/j.jallcom.2022.167478

[2] P. Samal, P. R. Vundavilli, A. Meher, M. M. Mahapatra, Recent progress in aluminum metal matrix composites: A review on processing, mechanical and wear properties, Journal of Manufacturing Processes 59 (2020) 131–152. https://doi.org/10.1016/j.jmapro.2020.09.010

[3] C. Zhu, Z. Wang, K. Zhou, Q. Wu, P. Zhao, X. Fan, J. Wang, Triple the ductility of as-cast Al-Si alloys by phase-selective recrystallization, Materials Science and Engineering A 855 (2022) 143902. https://doi.org/10.1016/j.msea.2022.143902

[4] M. Zamani, L. Morini, L. Ceschini, S. Seifeddine, The role of transition metal additions on the ambient and elevated temperature properties of Al-Si alloys, Materials Science and Engineering A 693 (2017) 42–50. https://doi.org/10.1016/j.msea.2017.03.084

[5] R. V. Reyes, T. S. Bello, R. Kakitani, T. A. Costa, A. Garcia, N. Cheung, J. E. Spinelli, Tensile properties and related microstructural aspects of hypereutectic Al-Si alloys directionally solidified under different melt superheat and transient heat flow conditions, Materials Science and Engineering A 685 (2017) 235–243. https://doi.org/10.1016/j.msea.2016.12.096

[6] A. Hekmat-Ardakan, X. Liu, F. Ajersch, X. G. Chen, Wear behaviour of hypereutectic Al-Si-Cu-Mg casting alloys with variable Mg contents, Wear 269 (2010) 684–692. https://doi.org/10.1016/j.wear.2010.07.007

[7] M. Goenka, C. Nihal, R. Ramanathan, P. Gupta, A. Parashar, J. Joel, Automobile parts casting – methods and materials used: A review, Materials Today: Proceedings 22 (2020) 2525–2531. https://doi.org/10.1016/j.matpr.2020.03.381

[8] P. Zhang, X. Nie, H. Hu, Y. Liu, TEM analysis and tribological properties of Plasma Electrolytic Oxidation (PEO) coatings on a magnesium engine AJ62 alloy, Surface and Coatings Technology 205 (2010) 1508–1514. https://doi.org/10.1016/j.surfcoat.2010.10.015

[9] P. Ma, Z. J. Wei, Y. D. Jia, Z. S. Yu, K. G. Prashanth, S. L. Yang, C. G. Li, L. X. Huang, J. Eckert, Mechanism of formation of fibrous eutectic Si and thermal conductivity of SiC_p/Al-20Si composites solidified under high pressure, Journal of Alloys and Compounds 709 (2017) 329–336. https://doi.org/10.1016/j.jallcom.2017.03.162

[10] X. Wang, C. Lu, W. Rao, Liquid metal-based thermal interface materials with a high thermal conductivity for electronic cooling and bioheat-transfer applications, Applied Thermal Engineering 192 (2021) 116937. https://doi.org/10.1016/j.applthermaleng.2021.116937

[11] L. G. Hou, C. Cui, J. S. Zhang, Optimizing microstructures of hypereutectic Al-Si alloys with high Fe content via spray forming technique, Materials Science and Engineering A 527 (2010) 6400–6412. https://doi.org/10.1016/j.msea.2010.06.066

[12] X. Y. Jiao, J. Wang, C. F. Liu, Z. P. Guo, G. D. Tong, S. L. Ma, S. M. Xiong, Characterization of high-pressure die-cast hypereutectic Al-Si alloys based on microstructural distribution and fracture morphology, Journal of Materials Science & Technology 35 (2019) 1099–1107. https://doi.org/10.1016/j.jmst.2018.12.005

[13] J. Abboud, J. Mazumder, Developing of nano sized fibrous eutectic silicon in hypereutectic Al-Si alloy by laser remelting, Scientific Reports 10 (2020) 12090. https://doi.org/10.1038/s41598-020-69072-1

[14] Q. Li, T. Xia, Y. Lan, W. Zhao, L. Fan, P. Li, Effect of rare earth cerium addition on the microstructure and tensile properties of hypereutectic Al-20%Si alloy, Journal of Alloys and Compounds 562 (2013) 25–32. https://doi.org/10.1016/j.jallcom.2013.02.016

[15] H. Xue, G. Lv, W. Ma, D. Chen, J. Yu, Separation mechanism of primary silicon from hypereutectic Al-Si melts under alternating electromagnetic fields, Metallurgical and Materials Transactions A 46 (2015) 2922–2932. https://doi.org/10.1007/s11661-015-2889-1

[16] J. H. Jeon, J. H. Shin, D. H. Bae, Si phase modification on the elevated temperature mechanical properties of Al-Si hypereutectic alloys, Materials Science and Engineering A 748 (2019) 367–370. https://doi.org/10.1016/j.msea.2019.01.119

[17] L. Zhu, F. Qiu, Q. Zou, X. Han, S. L. Shu, H. Y. Yang, Q. C. Jiang, Multiscale design of α-Al, eutectic silicon and Mg2Si phases in Al-Si-Mg alloy manipulated by in situ nanosized crystals, Materials Science and Engineering A 802 (2021) 140627. https://doi.org/10.1016/j.msea.2020.140627

[18] N. Kang, P. Coddet, H. Liao, T. Baur, C. Coddet, Wear behavior and microstructure of hypereutectic Al-Si alloys prepared by selective laser melting, Applied Surface Science 378 (2016) 142–149. https://doi.org/10.1016/j.apsusc.2016.03.221

[19] Y. Li, J. Liu, Q. Zhang, W. Huang, Casting defects and microstructure distribution characteristics of aluminum alloy cylinder head with complex structure, Materials Today Communications 27 (2021) 102416. https://doi.org/10.1016/j.mtcomm.2021.102416

[20] M. J. Park, H. So, L. Kang, J. W. Byeon, K. H. Kim, The relation between mechanical properties and microstructural evolution induced by Sc microalloying in Al-20Zn-3Cu alloy, Journal of Alloys and Compounds 889 (2021) 161719. https://doi.org/10.1016/j.jallcom.2021.161719

[21] M. E. Van Dalen, T. Gyger, D. C. Dunand, D. N. Seidman, Effects of Yb and Zr microalloying additions on the microstructure and mechanical properties of dilute Al-Sc alloys, Acta Materialia 59 (2011) 7615–7626. https://doi.org/10.1016/j.actamat.2011.09.019

[22] H. Zhang, H. Zhu, X. Nie, J. Yin, Z. Hu, X. Zeng, Effect of Zirconium addition on crack, microstructure and mechanical behavior of selective laser melted Al-Cu-Mg alloy, Scripta Materialia 134 (2017) 6–10. https://doi.org/10.1016/j.scriptamat.2017.02.036

[23] A. Martin, M. Vilanova, E. Gil, M. San Sebastian, C. Y. Wang, S. Milenkovic, C. M. Cepeda-Jiménez, Influence of the Zr content on the processability of a high strength Al-Zn-Mg-Cu-Zr alloy by laser powder bed fusion, Materials Characterization 183 (2022) 111650. https://doi.org/10.1016/j.matchar.2021.111650

[24] J. F. Leng, B. H. Ren, Q. B. Zhou, J. W. Zhao, Effect of Sc and Zr on recrystallization behavior of 7075 aluminum alloy, Transactions of Nonferrous Metals Society of China 31 (2021) 2545–2557. https://doi.org/10.1016/S1003-6326(21)65674-1
[25] D. Su, J. Zhang, B. Wang, The microstructure and weldability in welded joints for AA 5356 aluminum alloy after adding modified trace amounts of Sc and Zr, Journal of Manufacturing Processes 57 (2020) 488–498. https://doi.org/10.1016/j.jmapro.2020.07.017
[26] J. A. Glerum, A. De Luca, M. L. Schuster, C. Kenel, C. Leinenbach, D. C. Dunand, Effect of oxide dispersoids on precipitation-strengthened Al-1.7Zr (wt.%) alloys produced by laser powder-bed fusion, Additive Manufacturing 56 (2022) 102933. https://doi.org/10.1016/j.addma.2022.102933
[27] J. R. Croteau, S. Griffiths, M. D. Rossell, C. Leinenbach, C. Kenel, V. Jansen, N. Q. Vo, Microstructure and mechanical properties of Al-Mg-Zr alloys processed by selective laser melting, Acta Materialia 153 (2018) 35–44. https://doi.org/10.1016/j.actamat.2018.04.053
[28] A. S. Prosviryakov, K. D. Shcherbachev, Strengthening of mechanically alloyed Al-based alloy with high Zr contents, Materials Science and Engineering A 713 (2018) 174–179. https://doi.org/10.1016/j.msea.2017.12.069
[29] Q. B. Yang, Y. J. Deng, Y. A. N. G. Mou, Z. Q. Zhang, W. G. Li, L. I. U. Qing, Effect of Al3Zr particles on hot-compression behavior and processing map for Al-Cu-Li based alloys at elevated temperatures, Transactions of Nonferrous Metals Society of China 30 (2020) 872–882. https://doi.org/10.1016/S1003-6326(20)65261-X
[30] W. C. Tang, Z. Y. Piao, J. Zhang, S. Y. Liu, L. J. Deng, Effect of trace elements on the pinhole fatigue-resistance of gasoline Al-Si piston alloy, Engineering Failure Analysis 108 (2020) 104340. https://doi.org/10.1016/j.engfailanal.2019.104340
[31] J. Guo, Z. P. Guan, R. F. Yan, P. K. Ma, M. H. Wang, P. Zhao, J. G. Wang, Effect of modification with different contents of Sb and Sr on the thermal conductivity of hypoeutectic Al-Si alloy, Metals 10 (2020) 1637. https://doi.org/10.3390/met10121637
[32] C. Li, C. Wang, Z. Z. Yang, P. K. Ma, M. W. Ren, H. Y. Wang, Effect of complex modification of Ca and Sb on the microstructure and mechanical properties of hypoeutectic Al-11Mg2Si alloy, Journal of Alloys and Compounds 869 (2021) 159304. https://doi.org/10.1016/j.jallcom.2021.159304
[33] G. Mao, H. Yan, C. Zhu, Z. Wu, W. Gao, The varied mechanisms of yttrium (Y) modifying a hypoeutectic Al-Si alloy under conditions of different cooling rates, Journal of Alloys and Compounds 806 (2019) 909–916. https://doi.org/10.1016/j.jallcom.2019.07.107
[34] K. Nogita, H. Yasuda, M. Yoshiya, S. D. McDonald, K. Uesugi, A. Takeuchi, Y. Suzuki, The role of trace element segregation in the eutectic modification of hypoeutectic Al-Si alloys, Journal of Alloys and Compounds 489 (2010) 415–420. https://doi.org/10.1016/j.jallcom.2009.09.138
[35] E. M. Elgallad, H. W. Doty, S. A. Alkahtani, F. H. Samuel, Effects of La and Ce addition on the modification of Al-Si based alloys, Advances in Materials Science and Engineering 2016 (2016) 5027243. https://doi.org/10.1155/2016/5027243
[36] S. Hegde, K. N. Prabhu, Modification of eutectic silicon in Al-Si alloys, Journal of Materials Science 43 (2008) 3009–3027. https://doi.org/10.1007/s10853-008-2505-5
[37] F. Guo, W. Wang, W. Yu, Y. Zhang, S. Pan, Z. Zhou, X. Tian, Enhanced nucleation and refinement of eutectic Si by high number-density nano-particles in Al-10Si-0.5Sb alloys, Materials & Design 117 (2017) 382–389. https://doi.org/10.1016/j.matdes.2017.01.009
[38] C. Y. Yang, S. L. Lee, C. K. Lee, J. C. Lin, Effects of Sr and Sb modifiers on the sliding wear behavior of A357 alloy under varying pressure and speed conditions, Wear 261 (2006) 1348–1358. https://doi.org/10.1016/j.wear.2006.03.051
[39] J. D. Lin, P. Okle, D. C. Dunand, D. N. Seidman, Effects of Sb micro-alloying on precipitate evolution and mechanical properties of a dilute Al-Sc-Zr alloy, Materials Science and Engineering A 680 (2017) 64–74. https://doi.org/10.1016/j.msea.2016.10.067
[40] C. L. Pereira, L. F. Gomes, J. E. Spinelli, Effects of Bi addition on Si features, tensile properties and wear resistance of hypereutectic Al-15Si alloy, Materials Research 23 (2020). https://doi.org/10.1590/1980-5373-MR-2020-0107
[41] H. Mii, M. Senoo, I. Fujishiro, Solid solubility of Si in Al under high pressure, Japanese Journal of Applied Physics 15 (1976) 777–783. https://doi.org/10.1143/JJAP.15.777
[42] R. Haghayeghi, G. Timelli, An investigation on primary Si refinement by Sr and Sb additions in a hypereutectic Al-Si alloy, Materials Letters 283 (2021) 128779. https://doi.org/10.1016/j.matlet.2020.128779
[43] S. Z. Lu, A. Hellawell, The mechanism of silicon modification in aluminum-silicon alloys: Impurity induced twinning, Metallurgical Transactions A 18 (1987) 1721–1733. https://doi.org/10.1007/BF02646204
[44] O. Uzun, F. Yilmaz, U. Kölemen, N. Başman, Sb effect on micro structural and mechanical properties of rapidly solidified Al-12Si alloy, Journal of Alloys and Compounds 509 (2011) 21–26. https://doi.org/10.1016/j.jallcom.2010.09.037
[45] K. Gall, M. Horstemeyer, D. L. McDowell, J. Fan, Finite element analysis of the stress distributions near damaged Si particle clusters in cast Al-Si alloys, Mechanics of Materials 32 (2000) 277–301. https://doi.org/10.1016/S0167-6636(00)00003-X
[46] F. Yilmaz, R. Elliott, Halo formation in Al-Si alloys, Metal Science 18 (1984) 362–366. https://doi.org/10.1179/030634584790419935
[47] S. M. Lloyd, M. Babiker, G. Thirunavukkarasu, J. Yuan, Electron vortices: Beams with orbital angular momentum, Reviews of Modern Physics 89 (2017) 035004. https://doi.org/10.1103/RevModPhys.89.035004
[48] M. J. Peet, H. S. Hasan, H. K. D. H. Bhadeshia, Prediction of thermal conductivity of steel, International Journal of Heat and Mass Transfer 54 (2011) 2602–2608. https://doi.org/10.1016/j.ijheatmasstransfer.2011.01.025

[49] M. Lipińska, P. Bazarnik, M. Lewandowska, The influence of severe plastic deformation processes on electrical conductivity of commercially pure aluminium and 5483 aluminium alloy, Archives of Civil and Mechanical Engineering 16 (2016) 717–723. https://doi.org/10.1016/j.acme.2016.04.013

[50] M. Morozov, G. Y. Tian, P. J. Withers, Non-contact evaluation of the dependency of electrical conductivity on stress for various Al alloys as a function of plastic deformation and annealing, Journal of Applied Physics 108 (2010) 024909. https://doi.org/10.1063/1.3456996

[51] S. Karabay, Modification of AA-6201 alloy for manufacturing of high conductivity and extra high conductivity wires with property of high tensile stress after artificial aging heat treatment for all-aluminium alloy conductors, Materials & Design 27 (2006) 821–832. https://doi.org/10.1016/j.matdes.2005.06.005

[52] Y. Zhao, H. B. Liu, C. Y. Zhao, Experimental study on the cycling stability and corrosive property of Al-Si alloys as phase change materials in high-temperature heat storage, Solar Energy Materials and Solar Cells 203 (2019) 110165. https://doi.org/10.1016/j.solmat.2019.110165

[53] Z. Zhao, H. Xiang, H. Chen, F. Z. Dai, X. Wang, Z. Peng, Y. Zhou, High-entropy $(Nd_{0.2}Sm_{0.2}Eu_{0.2}Y_{0.2}Yb_{0.2})_4Al_2O_9$ with good high temperature stability, low thermal conductivity, and anisotropic thermal expansivity, Journal of Advanced Ceramics 9 (2020) 595–605. https://doi.org/10.1007/s40145-020-0399-0

[54] P. Wang, J. B. Li, R. N. Xu, P. X. Jiang, Non-uniform and volumetric effect on the hydrodynamic and thermal characteristic in a unit solar absorber, Energy 225 (2021) 120130. https://doi.org/10.1016/j.energy.2021.120130

[55] J. Li, X. Li, Y. Zheng, Z. Liu, Q. Tian, X. Liu, New underfill material based on copper nanoparticles coated with silica for high thermally conductive and electrically insulating epoxy composites, Journal of Materials Science 54 (2019) 6258–6271. https://doi.org/10.1007/s10853-019-03335-9

[56] H. A. Abdel-Aal, Temperature rise in sliding solids: Influence of contact pressure and temperature on thermal conduction, Tribology Letters 68 (2020) 1–20. https://doi.org/10.1007/s11249-020-1272-6

[57] F. Z. Akbarzadeh, M. Rajabi, Mechanical alloying fabrication of nickel/cerium/MgH_2 nanocomposite for hydrogen storage: Molecular dynamics study and experimental verification, Journal of Alloys and Compounds 899 (2022) 163280. https://doi.org/10.1016/j.jallcom.2021.163280